Development and validation of a simplified kinetic model for predicting organic micropollutant degradation in vacuum ultraviolet water treatment

N. Kovoor George [a,b,*], B.A. Wols [b,c], W. Gernjak [d,e]

[a] *University of Girona, Plaça de Sant Domènec, 3, 17004 Girona, Spain*
[b] *Wetsus, Leeuwarden 8911MA, the Netherlands*
[c] *KWR, Groningenhaven 7, 3433 PE Nieuwegein, the Netherlands*
[d] *Catalan Institute for Water Research (ICRA), 17003 Girona, Spain*
[e] *Catalan Institution for Research and Advanced Studies (ICREA), 08100 Barcelona, Spain*

A B S T R A C T

Vacuum-UV (VUV) advanced oxidation processes (AOPs) show promise for organic micropollutant (OMP) degradation, offering a chemical-free and cost-effective solution. Integrating VUV-AOP with conventional UV/H$_2$O$_2$ AOP can reduce H$_2$O$_2$ dosing. However, upscaling VUV-AOP faces challenges due to limited VUV photon penetration in water. Kinetic modelling is required to assess the feasibility of VUV AOPs for industrial water matrices. This paper presents a *quasi*-steady-state kinetic model, balancing simplicity with robustness. The model includes direct photolysis at UV$_{254nm}$ and VUV$_{185nm}$ and oxidation via hydroxyl, chlorine, and carbonate radicals as degradation pathways. The model is calibrated by including or excluding (photo)chemical reactions and simplified using steady-state assumptions for each relevant reactive radical. The model is validated against lab-scale experiments in Milli-Q® water, groundwater, surface water, and tap water matrices for carbamazepine, atrazine, and diclofenac. These compounds have varying degrees of direct photolysis and oxidation rates, thus validating the model's ability to predict their contributions toward organic micropollutant degradation. Surface water and tap water matrices are spiked with various anions the effect of which was well-predicted by the model. The model can be adapted for a computational fluid dynamics platform, accelerating reactor design.

1. Introduction

UV-advanced oxidation processes (AOPs) are a crucial barrier against organic micropollutants (OMPs) in various applications, including drinking water [1], wastewater applications [2], hospital wastewater [3], etc. The UV/H$_2$O$_2$ AOP is one of the most extensively utilised UV-AOPs [4], receiving considerable attention in studies concerning water reuse. In the UV/H$_2$O$_2$ AOP, UV photons at 254 nm generate hydroxyl radicals (HO·) through H$_2$O$_2$ homolysis (R1). However, the low molar absorption coefficient of H$_2$O$_2$ at UV$_{254nm}$, ε_{UV,H_2O_2} = 20 M^{-1}.cm^{-1}, [5] results in a diminished radical yield, elevated H$_2$O$_2$ consumption, and increased operational costs.

Within the UV/H$_2$O$_2$ AOP, UV irradiation is delivered through either medium-pressure (MP) or low-pressure (LP) UV lamps, both of which serve as mercury (Hg)-vapor-based UV sources. Notably, due to their superior efficiency in converting electricity to UV output LP-UV lamps require less electrical energy per order for degrading pesticides and

pharmaceuticals compared to MP-UV lamps [6]. LP-UV lamps generate vacuum UV (VUV) radiation at 185 nm alongside UV at 254 nm. Commercial LP-UV lamps equipped with synthetic quartz sleeves, known as "ozone-generating lamps", enable the permeation of VUV photons [7].

VUV$_{185nm}$ photons are efficiently absorbed by water molecules, generating non-selective and highly reactive hydroxyl radicals (HO·) through water photolysis (R2) and homolysis (R3), with quantum yields of 0.33 and 0.045, respectively. Therefore, combining VUV-AOP and conventional UV/H$_2$O$_2$ AOP could reduce the H$_2$O$_2$ required and thereby lessen the chemical cost to achieve the degradation of OMPs. Contrary to the poor absorbance of UV by H$_2$O$_2$, in VUV-AOP, *all* incident VUV photons are absorbed by water or other significant absorbers to generate radicals. Thus, the inherent efficiency of VUV-AOP is substantially higher than UV/H$_2$O$_2$ AOP.

Water absorbance was determined using the molar absorption coefficient of water at VUV$_{185nm}$, ε_{VUV,H_2O} = 0.0324 M^{-1}.cm^{-1} [5], and the water concentration, 55.55 M, is 1.76 cm^{-1}. This significant water

absorbance results in over 90% of VUV_{185nm} photons being absorbed within the initial 5–6 mm of the water sample. This poses a considerable challenge to scaling up VUV-AOPs.

Despite the challenge, studies are increasingly exploring VUV-AOPs as standalone [8,9,10] or integrated processes, such as VUV/O_3 in a continuous-flow fluidised bed reactor [11], VUV/UVC and VUV/H_2O_2 in a helical baffle reactor [12], VUV/PMS [13] and VUV integrated with granular-biofiltration [14]. In integrated AOPs, the additional HO· generated via the VUV/H_2O system allows for a reduction in oxidant quantity. Integrating VUV into UV-based AOPs employing LP-UV lamps incurs no additional electrical energy costs, as it is generated from the same source as UV. Standalone VUV-AOPs often report electrical energy per order (E_{EO}) values below $1 kWh.m^{-3}$ [15].

However, much of the existing literature focuses on lab-scale photoreactor experiments. Although VUV-AOPs have proven effective and matured at the laboratory scale, their potential must be explored in commercial applications. This is primarily due to halted progress in optimizing reactor parameters [16] and a lack of pilot-scale demonstrations showcasing their effectiveness, particularly in removing OMPs from natural water sources such as wastewater matrices [14]. Modelling VUV-based AOPs is crucial for expediting their scale-up. There are several works of literature pertaining modelling of VUV-AOPs. For example, S. Zhu et al., [17] developed a dynamic model predicting carbamazepine (CBZ) degradation in VUV-AOP within Milli-Q® water, accounting for natural organic matter (NOM) and varying CBZ concentrations. Similarly, a comprehensive model with 51 reactions was constructed to forecast the degradation of 1,4-Dioxane (1,4-D) and atrazine (ATZ) in Milli-Q® and natural waters. While extensive reaction schemes enhance accuracy in predicting OMP degradation, troubleshooting parameter deviations between model and experimental results can be laborious, limiting the practicality of such models, primarily to experts. And, while high accuracy is imperative in specific applications, such as ultra-pure water production in the semiconductor industry, a model predicting percentage removal of OMPs within ± 5–10 % of the experimental value is often deemed sufficient in drinking water treatment [18].

G. Shi et al., [16] illustrate applying a "grey-box kinetic model," balancing accuracy and simplicity in real-world scenarios. The model consolidates all scavenging into a unified term, calculating the dose-based degradation rate constant (k_{dose}, $m^2.J^{-1}$) of 1,4-D from batch experiments. The authors validated this simplified model by examining the parameter k_{dose} through experimental data. Subsequently, they implemented the "grey-box kinetic model" in Computational Fluid Dynamics (CFD) to project the 1,4-D degradation in annular photoreactors. While this approach proves practical and yields a straightforward kinetic model, its drawback lies in the need for batch experiments to determine k_{dose} for specific settings, including OMP type, water matrix, and H_2O_2 dosing. P. Xie et al., [19] propose a more complicated kinetic model, accounting for significant degradation pathways such as direct photolysis at UV_{254nm} and oxidation via hydroxyl radicals (HO·). This model accurately predicts the degradation of benzoic acid, bisphenol-A, nitrobenzene, and dimethyl phthalate in natural waters. However, it is unsuitable for VUV-AOP in scenarios where chloride (Cl^-) chemistry plays a pivotal role, as demonstrated by the low chloride content (8.5 and 10.3 mg. L^{-1}) in the studied waters A and B.

Thus, for OMP degradation in VUV-AOPs, there is a demand for simple, robust kinetic models. Our study proposes a quasi-Steady-State (SS) kinetic model incorporating photolysis and oxidation via HO·, Cl·, CO_3^- pathways for OMP degradation. SS kinetic models, recognized for their simplicity and utility, have successfully predicted OMP degradation in various AOPs like UV/H_2O_2, UV/O_3, and UV/PMS [20,21,22]. Modelling OMP degradation in natural water matrices proves challenging due to the complex composition of components such as Cl^-, Br^-, NO_3^-, SO_4^{2-}, $H_2CO_3/HCO_3^-/CO_3^{2-}$, DOC, and OMPs, where OMPs are in micromolar concentration levels. These components instigate multiple reactions that generate or scavenge oxidizing or reducing radicals, with matrix and OMP-specific effects. AOP efficacy depends not only on

radical generation but also on their availability for OMP oxidation [23]. Our study carefully selects reactions and reactive species in natural waters to avoid unnecessary complexity in the kinetic model. The model is applied to predict the degradation of carbamazepine (CBZ), atrazine (ATZ), and diclofenac (DCF) in diverse water matrices. The concept of "useful absorbed energy" (uAE), derived from our previous work [24], is used in the model.

2. Materials and methods

2.1. Experimental reactor configuration

The qCB apparatus (see Fig. S1) consisted of a lamp housing and a collimator, both purged with nitrogen gas to prevent the formation of ozone which would otherwise be formed when VUV is absorbed by atmospheric oxygen [25]. The qCB apparatus was equipped with a 22.5 W LP-Hg lamp (emitting UV_{254nm} and VUV_{185nm} irradiation). A 33 cm distance between the lamp's center and the sample's surface was maintained based on a Petri factor of 0.97 [26]. The diameter of the collimator was 5 ± 0.5 cm. The outlet of the collimator was equipped with a shutter, which was closed after each irradiation experiment with an accuracy of ± 5 s. A closed cylindrical quartz cell (type 35/Q, Starna Scientific, Germany) was filled with sample, placed directly under the collimator, and continuously stirred. A 1 cm or 2 cm physical path length cell was used depending on the experiment's requirement. The effective path length of VUV varied from 0.02 cm in the surface water matrix to 0.24 cm in the RO permeate. The effective path length of UV varied from 1.6 cm in tap water matrix to 2 cm in Milli Q® (see Text S1 for calculation of effective pathlength). IL1700 radiometer employing the SED254/NS254 and SED185/NS185 detectors (International Light Technologies Inc., Massachusetts) measured the UV_{254nm} and VUV_{185nm} irradiations, respectively. The photon flux density received by the samples varied slightly per experiment and was ~ 0.06 $\mu Einstein.L^{-1}.sec^{-1}$ at 185 nm and ~ 0.5 $\mu Einstein.L^{-1}.sec^{-1}$ at 254 nm. The respective incident irradiations were in the range of 0.33 $W.m^{-2}$ and 2.6 $W.m^{-2}$.

During $VUV+UV/H_2O_2$ AOP and VUV+UV AOP experiments, the sample with and without H_2O_2 was placed under the qCB setup and irradiated. In the case of UV/H_2O_2 AOP experiments, a closed cylindrical quartz cell (1 cm) filled with 4 M NaCl was placed on top of the sample cell to block VUV_{185nm}. This arrangement also reduced 23 % of incident UV_{254nm} irradiation, which was accounted for in the results analyses.

2.2. Chemicals and analyses

Water matrices used in this study were Milli-Q®, reverse osmosis permeate (RO), drinking water sourced from surface water (Lake IJssel, the Netherlands) with high chloride content (SW), drinking water sourced from groundwater with low chloride content (GW) and tap water matrix (see Table 1 for quality of water matrices). Anions and cations were measured using ion chromatography using a Thermo Scientific Dionex Aquion with a Dionex Ionpac AS22 RFIC column and Dionex Ionpac AG22 RFIC pre-column. Total (in)organic carbon was measured using a Shimadzu TOC-L TOC analyzer. Liquid chromatography-mass spectrometry (LC-MS) was used to measure OMP concentrations. The LC was outfitted with an Agilent Zorbax Eclipse Plus C18 RRHD (1.8 μm, 50*2.1 mm) column, equipped with a UHPLC guard Zorbax Eclipse Plus C18 (1.8 μm, 2.1*5mm) pre-column. The flow rate was set at 0.25 mL min^{-1}, and the column temperature was maintained at 40 °C. For the MS, an Agilent 6420 Triple Quadrupole (QqQ) Mass Analyzer with an electrospray ion source was used. CBZ, DCF, and t-BuOH were bought from Sigma Aldrich. ATZ and DCF were bought from VWR Chemicals. These chemicals were used as purchased.

The UV_{254nm} absorbance is measured using a spectrophotometer. VUV_{185nm} absorbance is estimated as the sum of the products of molar absorption coefficients and concentrations of H_2O, Cl^-, NO_3^-, HCO_3^-, and SO_4^{2-}.

Table 1
Quality parameters of various water matrices experimented.

	Unit	Milli-Q®	RO	SW	GW	Tap Water
DOC	mg. L^{-1}	8.6–16.1*	0.5**	1.1	1.3	3.5
pH			6.2	7.1	8.0	7.7
Cl$^-$	mg. L^{-1}		32.7	168	9.3	53.3
NO$_3^-$	mg. L^{-1}		3.3	1.3	0.7	9.9
SO$_4^{2-}$	mg. L^{-1}		0.6	64.2	0.8	1.3
HCO$_3^-$	mg. L^{-1}		8.2	94.5	157	244
CO$_3^{2-}$	mg. L^{-1}		5.61E-04	0.05	0.7	0.7
Br-	mg. L^{-1}		< 0.10	0.30	< 0.10	–
absorbance UV$_{254nm}$	cm^{-1}		0.00	0.05	0.05	0.1
absorbance VUV$_{185nm}$	cm^{-1}		5.7	12.6	4.0	9.5

*Added as tertiary butanol.
**Half of the limit of quantification value.

3. Kinetic model

The kinetic model is calibrated by including only relevant reaction schemes and reactive species. The approach used to develop the kinetic model is as follows: firstly, the reaction schemes and reactive species widely known to affect AOP performance are collected from the literature. Next, their practical relevance was assessed based on experimental observations reported in the literature. In the sections that follow, concise discussions of the assessments are given. More detailed discussions are provided in the supplementary information. Sections 4.1.1 and 4.1.2 assess the relevance of photoproducts formed under UV$_{254nm}$ and VUV$_{185nm}$ irradiation, respectively. Section 4.1.3 outlines the significance of various scavengers for HO·, Cl· and CO$_3^-$ radicals. A detailed examination of the aspects is given in Text S3-Text S5.

3.1. Model description

3.1.1. Reaction scheme for Milli-Q® water

Table 2 gives the reactions included in the kinetic model for predicting OMPs' degradation in Milli-Q® water spiked with a scavenger.

When a VUV photon is absorbed by H$_2$O, it can trigger either R2 or R3, or it may not cause any reaction. On average, for every mole of VUV photons absorbed by H$_2$O, 0.33 and 0.045 mol of HO· are generated via R2 and R3, respectively. And hence, their contribution to contaminant is additive. In the simplified kinetic model developed in this study, R2 and R3 are summed into a single equation where the quantum yield of HO· is $\Phi_{HO}^{R3} = 0.375$. Imoberdorf et al., employed the addition of quantum yields of HO· production for the kinetic modelling for degradation of 1,4-Dioxane under vacuum-UV irradiation [27]. Due to its lower generation rate, contributions of $H·$ and e_{aq}^- are not included in the model. The target OMP and scavenger used to validate this kinetic model are CBZ and t-BuOH with $k_{R8} = 9.5\text{x}10^9$ M^{-1}.s^{-1} [28] and $k_{R9} = 5\text{x}10^8$ M^{-1}.s^{-1} [29]. Direct photolysis of t-BuOH by VUV is not included due to its low molar absorption coefficient (72.8 M^{-1}.cm^{-1}) [30].

Table 2
Reactions in the kinetic model for OMP degradation in Milli-Q® water.

Reaction	Reaction rates	Reference	#
$H_2O_2 + h\nu_{254nm} \rightarrow 2HO·$	$\Phi_{HO}^{R1} = 1$ $\varepsilon_{UV,H_2O_2} = 19.9$ M^{-1}.cm^{-1}	[69]	(R1)
$H_2O + h\nu_{185nm} \rightarrow HO· + H·$	$\Phi_{HO}^{R2} = 0.33$ $\varepsilon_{VUV,H_2O} = 0.0324$ M^{-1}.cm^{-1}	[70,5]	(R2)
$H_2O + h\nu_{185nm} \rightarrow HO· + H^+ + e_{aq}^-$	$\Phi_{HO}^{R3} = 0.045$	[70]	(R3)
$H_2O_2 + h\nu_{185nm} \rightarrow 2HO·$	$\Phi_{HO}^{R4} = 1$ $\varepsilon_{VUV,H_2O_2} = 289$ M^{-1}.cm^{-1}	[71]	(R4)
$OMP + h\nu_{254nm} \rightarrow products$			(R5)
$OMP + h\nu_{185nm} \rightarrow products$			(R6)
$H_2O_2 + HO· \rightarrow products$	$2.7 \times 10^7 M^{-1}.s^{-1}$	[71]	(R7)
$targetOMP + HO· \rightarrow products$	k_{R8}		(R8)
$Scavenger + HO· \rightarrow products$	k_{R9}		(R9)

3.1.2. Reaction scheme for natural water matrices

In addition to the reactions in Table 2, reactions in Table 3 are included for modelling OMP degradation in natural waters. Table 4 shows the photo-chemical constants of CBZ, ATZ, and DCF used in the kinetic model. The rationale behind the choices of these reactions and reactive species is described in Section 4.1.

3.2. Methodology to solve the kinetic model

The primary goal of the kinetic model is to predict OMP degradation in a specific water matrix. To calculate the OMP degradation, steady-state concentrations of HO· and Cl· (Eq. (1)) are first calculated. These concentrations would depend on their generation and consumption rates and will be specific for each water matrix.

$$[X·]_{ss} = \frac{1}{t * \sum_{i=1}^{n} k_{S_i,X·} * [S_i]} \sum_{C,\lambda} \frac{uAE_\lambda * f_{\lambda,C} * \Phi_{C,\lambda}^{Rx}}{U_\lambda} \quad (1)$$

where X· = HO· or Cl·; t is the time of irradiation in s; $k_{S_i,X}$, second-order reaction rate constant (in M^{-1}s^{-1}) between the ith scavenger, S_i and n is the total number of scavengers; λ = UV$_{254nm}$ and VUV$_{185nm}$; C= H$_2$O$_2$, H$_2$O and Cl$^-$; uAE_λ is the useful absorbed energy in J.m^{-3}; Φ_X^R is the quantum yield of X· from reaction R (Table 2 and Table 3); $f_{\lambda,C}$ is the fraction of λ photons absorbed by the oxidant, C, relative to the total absorption; U_λ is the energy per mole λ in J.mol^{-1}. Useful absorbed energy refers to the portion of energy introduced into the fluid absorbed by the constituents in the water sample, triggering the formation of reactive radicals. It is a novel concept which was introduced in [24].

The steady-state concentration of CO_3^- is calculated as the ratio of the formation of CO_3^- by the reaction of $[HO·]_{ss}$ and $[Cl·]_{ss}$ with carbonate species and scavenging of CO_3^- to its consumption by scavengers (Eq. (2)).

$$[CO_3^-]_{ss} = \frac{1}{\sum_{i=1}^{n} k_{S_i,CO3^-} * [S_i]} * \sum_{C,\lambda} k_{X·,C} * [X·]_{ss} * C \quad (2)$$

where C=CO$_3^{2-}$ and HCO$_3^-$ and S_i = DOC and H$_2$O$_2$

Finally, the sum of the products of $k_{OMP,X·}$ and the model predicted $[X·]_{ss}$ and irradiation time results in the natural logarithmic degradation of OMP, $ln\left(\frac{[OMP]_t}{[OMP]_0}\right)$ via radical oxidation. Direct photolysis of OMP under irradiation ($DP_{OMP,UV}$ and $DP_{OMP,VUV}$) is added to the contribution via radical oxidation, resulting in the equation for the total degradation of OMP as shown below:

$$ln\left(\frac{[OMP]_t}{[OMP]_0}\right) = -\left(\left(\sum_{X·} k_{OMP,X·} * [X·]_{ss}\right) + \sum_\lambda DP_{OMP,\lambda}\right) * t \quad (3)$$

Table 3
Reactions included in the kinetic model for OMP degradation in natural water.

Reaction	Reaction rates	Reference	#
$Cl^- + h\nu_{185nm} \rightarrow Cl·$	$\Phi_{Cl·}^{R10} = 0.4$ $\varepsilon_{VUV,Cl^-} = 3800 \pm 300$ M^{-1}.cm^{-1}	[72]	(R10)
$HCO_3^- + HO· \rightarrow CO_3^-$	$8.5 \times 10^6 M^{-1}.s^{-1}$	[73]	(R11)
$CO_3^{2-} + HO· \rightarrow CO_3^-$	$3.9 \times 10^8 M^{-1}.s^{-1}$	[74]	(R12)
$Br^- + HO· \rightarrow products$	$1.1 \times 10^{10} M^{-1}.s^{-1}$	[48]	(R13)
$DOC + HO· \rightarrow products$	k_{R14}(Table 6)		(R14)
$HCO_3^- + Cl· \rightarrow CO_3^-$	$2.2 \times 10^8 M^{-1}.s^{-1}$	[55]	(R15)
$CO_3^{2-} + Cl· \rightarrow CO_3^-$	$5.0 \times 10^8 M^{-1}.s^{-1}$	[47]	(R16)
$Br^- + Cl· \rightarrow products$	$1.2 \times 10^{10} M^{-1}.s^{-1}$	[48]	(R17)
$DOC + Cl· \rightarrow products$	k_{R18}(Table 6)	[55]	(R18)
$targetOMP + Cl· \rightarrow products$	k_{R19}		(R19)
$Scavenger + Cl· \rightarrow products$	k_{R20}		(R20)
$targetOMP + CO_3^- \rightarrow products$	k_{R21}		(R21)
$Scavenger + CO_3^- \rightarrow products$	k_{R22}		(R22)
$DOC + CO_3^- \rightarrow products$	k_{R23}(Table 6)		(R23)

Table 4
Photochemical constants of CBZ, ATZ, and DCF were used in the kinetic model.

	CBZ	ATZ	DCF
k_{HO} $(M^{-1}s^{-1})$	9.5×10^9 [28]	2.4×10^9 [75]	1.4×10^{10} [76]
k_{Cl} $(M^{-1}s^{-1})$	3.3×10^{10} [77]	6.9×10^9 [78]	3.8×10^{10} [77]
$k_{CO_3^-}$ $(M^{-1}s^{-1})$	4.5×10^7 [79]	3.7×10^7 [67]	8×10^7
Φ_{254}	6.0×10^{-3} [80]	4.8×10^{-2} [75]	3.8×10^{-1} [81]
$\varepsilon_{254} (M^{-1}cm^{-1})$	6070 [80]	3860 [75]	6140
Φ_{185}	n.a	4.6×10^{-2} [82]	3.8×10^{-1}
$\varepsilon_{185} (M^{-1}cm^{-1})$	n.a	25,370 [31]	11,502

where $[X^{\cdot}]_{ss} = [HO^{\cdot}]_{ss}, [Cl^{\cdot}]_{ss}, [CO_3^{\cdot-}]_{ss}$

A detailed description of the derivation is given in Text S2.

4. Results and discussion

4.1. Model calibration

4.1.1. Photoproducts of natural water matrix components under UV_{254nm} irradiation

In real water matrices, among the various inorganic ions and carbon sources, only dissolved (DOM) organic matter and NO_3^-/NO_2^- are known to absorb UV_{254nm} photons in a quantifiable manner [31,32].

- Photoproducts of NO_3^- photolysis at $UV_{254\ nm}$

At $UV_{254\ nm}$, NO_3^- photolysis ($\varepsilon_{UV,NO_3^-} = 3M^{-1}cm^{-1}$) [33] primarily leads to forming peroxynitrite ($\Phi_{ONOO^-} = 0.1$), nitrite ion ($\Phi_{NOO^-} = 0.01$) and $HO^{\cdot}$ ($\Phi_{HO^{\cdot}} = 0.09$)[34]. Even at the highest concentration tested in this study (9.9 mg. L^{-1}, as indicated in Table 1), the absorbance of NO_3^- by $UV_{254\ nm}$ photons is 5e-04 cm^{-1}, which is negligible compared to the absorbance of 7 mg.L^{-1} of H_2O_2 ($4x10^{-2}$ cm^{-1}). Consequently, the contribution of radicals generated via NO_3^- photolysis is excluded from the kinetic model. The absorption spectra of NO_2^- nearly overlap with that of NO_3^- in the UV region [35], and its quantum yield of $HO^{\cdot}$ generation is, $\Phi_{HO^{\cdot}} = 0.046$ [33], the photoproducts of NO_2^- are also excluded from the kinetic model, following the same rationale as for NO_3^- photoproducts.

- Photoproducts of DOM photolysis at $UV_{254\ nm}$

Photo-oxidation of organic matter generates triplet state DOM ($^3DOM^*$), singlet oxygen ($^1O_2$), and H_2O_2, all of which can interfere with OMP degradation [36]. However, $^3DOM^*$ was found to impact the OMP degradation only at UV doses in the range of 2000 mJ.cm^{-2} [37] (which is more than an order of magnitude higher than the doses applied in the current study) and is therefore excluded from the kinetic model.

4.1.2. Photoproducts of natural water matrix components by VUV_{185nm}

Even though all major anions absorb VUV_{185nm} photons [38], literature values of H_2O, Cl^-, NO_3^-, HCO_3^- and SO_4^{2-} were only available (Table 5).

- Photoproducts of Cl^- photolysis at $VUV_{185\ nm}$

In the water matrices considered in this study, due to their relatively high concentrations, only Cl^- and HCO_3^- (besides H_2O) significantly absorb VUV_{185nm} photons (R10), generating $Cl^{\cdot}$ radicals. $Cl^{\cdot}$ are comparable to $HO^{\cdot}$ in their reactivity but are more selective [39]. At a concentration of 0.6 mM, Cl^- absorbs equally as water in VUV_{185nm} AOP. Therefore, the photoproduct of Cl^-, $Cl^{\cdot}$, is included in the kinetic model.

- Photoproducts of NO_3^- photolysis at $VUV_{185\ nm}$

NO_3^- ions effectively absorb VUV_{185nm} photons generating NO_2^- via a complex set of pathways [40]. NO_2^- can scavenge both $HO^{\cdot}$ and $Cl^{\cdot}$ with rate constants, $1.1x10^{10}$ $M^{-1}s^{-1}$ and $5x10^9 M^{-1}s^{-1}$ [41], respectively. Despite having a higher molar absorption coefficient ($\varepsilon_{VUV,NO_3^-} = 4337 M^{-1}cm^{-1}$) than H_2O and Cl^-, due to the low concentrations of NO_3^-, the fraction of photons absorbed by NO_3^- is negligible (Table 5). Consequently, NO_2^- generation is insignificant and excluded from the kinetic model; nevertheless, in NO_3^- rich water, including NO_2^- as a $HO^{\cdot}$ and $Cl^{\cdot}$ scavenger must be considered.

- Photoproducts of SO_4^{2-} photolysis at $VUV_{185\ nm}$

Similarly, SO_4^{2-} ions absorb VUV_{185nm} photons generating $SO_4^{\cdot-}$, a strong oxidant (2.5–3.1 V) with a quantum yield of generation ≈ 0.7 [42]. However, even at a concentration of 200 mg. L^{-1}, VUV_{185nm} photons absorbed by SO_4^{2-} are less than 10% of that absorbed by water (1.76 cm^{-1}) and are therefore not included in the kinetic model.

- Photoproducts of HCO_3^- photolysis at $VUV_{185\ nm}$

Among the carbonate species, HCO_3^- has a low molar absorption coefficient (Table 5). In waters with low Cl^- content and pH between 6–8, a fraction of VUV_{185nm} photon absorbed by HCO_3^- could be significant, and thereby, its photoproduct $CO_3^{\cdot-}$ may become substantial (GW in Table 5). Unfortunately, since the quantum yield of $CO_3^{\cdot-}$ formation is unavailable, it has not been included in the kinetic model.

- Photoproducts of DOC photolysis at $VUV_{185\ nm}$

The molar absorption coefficient of DOC at VUV_{185nm} is unknown and depends on DOC composition. However, in natural water matrices, H_2O and Cl^- are assumed to be the major absorbers of VUV_{185nm} photons. Imoberdorf et al., [43] concludes that more than 99% of the VUV photons are absorbed by water in the presence of 4.5 mg.L^{-1} of total organic carbon. In any case, the generated excited-state DOC, the singlet oxygen species generated from it [44], is expected to affect the OMP degradation only negligibly compared to the contributions of $HO^{\cdot}$, $Cl^{\cdot}$, and $CO_3^{\cdot-}$ [45]. Therefore, these species are not included in the model.

4.1.3. Scavenging of $HO^{\cdot}$ And $Cl^{\cdot}$ By natural water matrix constituents

- Scavenging of $HO^{\cdot}$ and $Cl^{\cdot}$ by halide ions

Cl^- and Br^- react with $HO^{\cdot}$ following the scheme R24 [46], which is pH and halide concentration dependent. Extensive reaction schemes are outlined in other studies [47,48].

$$X^- + HO^{\cdot} \underset{R24_f}{\overset{R24_b}{\rightleftarrows}} HOX^{-\cdot} \tag{R24}$$

For Cl^-, $R24_b$ (4.3×10^9 $M^{-1}s^{-1}$ [49]) > $R24_f$ (6.9×10^9 $M^{-1}s^{-1}$ [49]), which is generating $HO^{\cdot}$. At neutral pH up to $[Cl^-] = 50$ mM, Y. Li et al., [50] observed no impact of Cl^- on the $[HO^{\cdot}]_{ss}$ in line with the findings in [51,52]. In this study, the highest concentration of Cl^- is 9.9

Table 5
Fraction of VUV_{185nm} photons absorbed by various anions in the three water matrices experimented.

Anion	$\varepsilon_{VUV}(M^{-1}.cm^{-1})$	Tap water	RO	SW	GW
H_2O	0.0324 [70,5]	19 %	32 %	9 %	49 %
Cl^-	3800 ± 300 [72]	61 %	62 %	87 %	27 %
SO_4^{2-}	200 [42]	0.04 %	3 %	0.01 %	0 %
NO_3^-	4337.1 This study	7 %	4 %	0 %	1 %
HCO_3^-	314.78 This study	12 %	1 %	2 %	20 %
H_2O_2	289 [71]	1 %	2 %	0 %	3 %

mM. Thus, Cl^- is *not* considered a scavenger of HO· in the kinetic model.

In the case of Br^-, R24 generates Br·$^-$, which reacts slowly with organic molecules [47]. J.E. Grebel *et al.,* [53] reports a reduction in phenol degradation due to Br·$^-$. Therefore, in the kinetic model, Br·$^-$ *is* considered a scavenger of HO·.

Cl^- and Br^- react with Cl· following the scheme R25. For Cl^-, the forward reaction, R25$_f$ (8.5×10^9 $M^{-1}s^{-1}$ [54]) has a higher reaction rate constant than the backward reaction, R25$_b$ (6.0×10^4 $M^{-1}s^{-1}$ [54]), resulting in Cl_2^- generation. Cl_2^- reacts with HCO_3^- (8×10^7 $M^{-1}s^{-1}$(B. M. [47]) and CO_3^{2-} (1.6×10^8 $M^{-1}s^{-1}$ (B. M. [47]), generating CO_3^-, which degrades OMPs. However, in some studies [55,56] negligible impact of Cl_2^- at Cl^- levels up to 20 mM on OMP degradation in UV/chlorine AOP was observed, indicating that the contribution of Cl_2^- is negligible for Cl^- levels of interest in drinking water applications. The highest concentration of chloride applied in this study was 9.9 mM. Hence, reaction R25 is not included in the kinetic model. However, the model allows the scavenging of Cl·, the Cl· That would have otherwise been scavenged by Cl^-, by carbonate species (see text below on Scavenging of HO· and Cl· by HCO_3^- and CO_3^{2-} ion).

$$X^- + Cl^· \underset{R25_f}{\overset{R25_b}{\rightleftharpoons}} XCl^· \tag{R25}$$

For Br^-, R25$_f$ (1.2×10^{10} $M^{-1}s^{-1}$ [47])> R25$_b$ (1.9×10^3 $M^{-1}s^{-1}$ [57]), which is generating BrCl·$^-$. BrCl·$^-$ contributes negligibly to OMP degradation. J.E. Grebel et al., [53] observed that BrCl·$^-$ contributed only around 2.5 % to the total phenol degradation even though the $[Cl^-]$ and [Br-] concentrations used were at least 50 times and 10 times higher than in this study. Hence Br- is considered as a scavenger of Cl·.

- Scavenging of HO· and Cl· by HCO_3^- and CO_3^{2-} ions

HCO_3^- and CO_3^{2-} reacts with HO· and Cl· generating CO_3^- (R11, R12, R15 and R16 in Table 3). CO_3^- is a highly selective radical ([58]; its reactivity with OMPs ranges from 10^2-10^9 M^{-1} [59]. CO_3^- has low reactivity with anions, and DOC is the major sink [59]. Consequently, CO_3^- achieves steady-state concentrations that are comparable to or higher than HO· and Cl·, compensating for its low reactivity with OMPs [60]. S. Zhu *et al.,* [17] and S. Yan *et al.,* [59], observed CO_3^- concentrations of $\approx 10^3$ and $\approx 10^2$ higher than HO· in UV/H$_2$O$_2$ AOP when 1–2 mM HCO_3^- was present and in sun-lit surface water, respectively. Therefore, HCO_3^- and CO_3^{2-} are considered as sources of CO_3^-.

- Scavenging of HO· and Cl· by NO_3^- ions

Scavenging of HO· by NO_3^- is excluded from the kinetic model because of its low reaction rate, $k_{HO·,NO_3^-} = 10^5 M^{-1}s^{-1}$. NO_3^- reacts with Cl· at $k_{Cl·,NO_3^-} = 1 \times 10^8 M^{-1}s^{-1}$[41]. Yet it is lower than Cl· reactivity with DOC, HCO_3^- and CO_3^{2-} (Table 3), which are in higher concentrations in natural water matrices. Thus, NO_3^- is an insignificant Cl· scavenger excluded from the kinetic model. NO_2^- has high reactivity with HO· and Cl· ($\approx 10^9 M^{-1}s^{-1}$), yet because of its low concentration, NO_2^- is not included in the model.

- Scavenging of HO· and Cl· by SO_4^{2-} ions

SO_4^{2-} reacts with HO· and Cl· generating SO_4^-, which could contribute positively towards the degradation of OMPs, especially electron-rich moieties [61]. However, due to its low concentrations, SO_4^- is not included in the model.

- Scavenging of HO· and Cl· by DOC

DOC scavenges HO· at a reaction rate, $k_{DOC,HO·}$, in the range of $1.4 \pm 0.2 \times 10^8$ to $(4.5 \pm 0.5) \times 10^8$ $M_C^{-1}s^{-1}$, and exceeding 10^9 $M_C^{-1}s^{-1}$ for effluent organic matter [62,63,64,65]. $k_{DOC,Cl·}$ varies in the range of 10^8-

10^9 $M_C^{-1}.s^{-1}$ [66]. In this study, $k_{DOC,HO·}$ value of 4.0×10^8 $M_C^{-1}s^{-1}$ was used for the RO, GW and SW water matrices, to render the model conservative (Table 6). $k_{DOC,HO·} = 4.0 \times 10^8$ $M_C^{-1}s^{-1}$, is also the value used often in literature. Relatively lower $k_{DOC,HO·}$ was used for tap water because it was known that the pre-treatment removed its aromatic DOC content. Literature reports a correlation between DOC and SUVA$_{254}$ [36], yet this study found none. Y. Lei *et al.,* [66] compares $k_{DOC,HO·}$ and $k_{DOC,Cl·}$ for 7 water types, resulting in $\left(\frac{k_{DOC,Cl·}}{k_{DOC,HO·}} \right)_{average} = 2.5$. This factor is used to estimate $k_{DOC,Cl·}$ in this study (Table 6). k_{DOC,CO_3^-} varied between 10^5-10^6 $M_C^{-1}s^{-1}$ [67,59], with no correlations found between k_{DOC,CO_3^-} and $k_{DOC,Cl·}$ and $k_{DOC,Cl·}$ conservatively, a value found in the higher end of the range in literature, $k_{DOC,CO_3^-} = 1 \times 10^6$ $M_C^{-1}.s^{-1}$, was used in the model.

4.2. Model validation

4.2.1. Model validation in Milli-Q® water

CBZ removal in Milli-Q® water spiked with t-BuOH is shown in Fig. 1 for VUV AOP, UV/H$_2$O$_2$ AOP, and VUV+UV/H$_2$O$_2$ AOP in 1 cm and 2 cm path length cells. After 10 min of irradiation in a 2 cm cell, CBZ removal was 24 % lower in UV/H$_2$O$_2$ AOP compared to a 1 cm cell. In the case of VUV+UV/H$_2$O$_2$ AOP, CBZ removal was, however, 40% lower in a 2 cm cell compared to a 1 cm cell. Hence, the effect of path length is more significant in VUV-based AOPs, which is explained by uAE. Doubling the path length resulted in only an 8% decrease in uAE for UV, while a substantial 49% decrease was observed for the uAE for VUV. A detailed discussion of the effect of path length is given in [24]. Close predictions by the model show that the path length effects are accounted for.

The effects of [t-BuOH] on CBZ removal in VUV and UV/H$_2$O$_2$ AOP are presented in Fig. 2. In line with the experiments, the model predicts decreasing degradation with increasing [t-BuOH]. The observed decrease in degradation is attributed to heightened scavenging of HO· with increasing t-BuOH concentrations.

4.2.2. Model validation in reverse osmosis (RO) permeate

OMP degradation in RO permeate was accurately predicted (Fig. 3). Despite high $[Cl^-]$, VUV AOPs exhibited high efficiency, indicating that Cl^- acts as a promoter by generating Cl·. Notably, $[Cl^-]$ is unusually high in RO water used in this study, and it was because of the operational issues with the RO membrane. Modelling revealed that $[HO·]_{ss}$, $[Cl·]_{ss}$ and $\left[CO_3^-\right]_{ss}$ are the highest in RO permeate among the water matrices tested in this study (Figure S 2 in SI). Consequently, the OMP removal efficiency was highest in the RO permeate. The high radical concentration is due to lower scavenger concentrations in RO permeate.

4.2.3. Model validation in groundwater matrix

CBZ and ATZ removals in groundwater were well-predicted by the model for all three AOPs (Fig. 4). The underestimation of CBZ and ATZ removals in VUV AOP is attributed to the exclusion of CO_3^- generated from the photolysis of HCO_3^- by VUV$_{185nm}$ irradiation in the kinetic model (section 4.1.2). In the groundwater matrix, about 20 % of VUV$_{185nm}$ photons are absorbed by HCO_3 (Table 5) generating CO_3^- radicals. CO_3^- has a considerable second-order reaction rate with CBZ and ATZ (Table 4).

DCF removal could have been better predicted by the VUV and VUV+UV/H$_2$O$_2$ AOP models. Since DCF degradation in UV/H$_2$O$_2$ AOP was nearly accurately predicted, the deviation comes from overestimating DCF degradation in VUV AOP. VUV$_{185nm}$ irradiation of complex water matrices generates a cocktail of oxidative and reductive radicals. DCF is extremely sensitive to oxidation [68], and underestimating/overestimating radical contribution might have led to the deviation.

Table 6

Values of $k_{DOC,HO}$, $k_{DOC,Cl}$ and k_{DOC,CO_3^-} used in the kinetic model. $k_{DOC,HO}$ values are determined as fitting parameters in UV/H$_2$O$_2$ AOP.

	SUVA$_{254}$ (cm^{-1}.mgC^{-1}.L)	$k_{DOC,HO}$ ($M_C^{-1}s^{-1}$)	$k_{DOC,Cl}$ ($M_C^{-1}s^{-1}$)	k_{DOC,CO_3^-} ($M_C^{-1}s^{-1}$)
RO	0.2*	4x10^8	1x10^9	1x10^6
Tap water	1.8	1.5x10^8	3.8 x10^8	1x10^6
GW	1.5	4x10^8	1x10^9	1x10^6
SW	2.2	4x10^8	1x10^9	1x10^6

*DOC value is assumed as half of the minimum limit of quantification (Table 1).
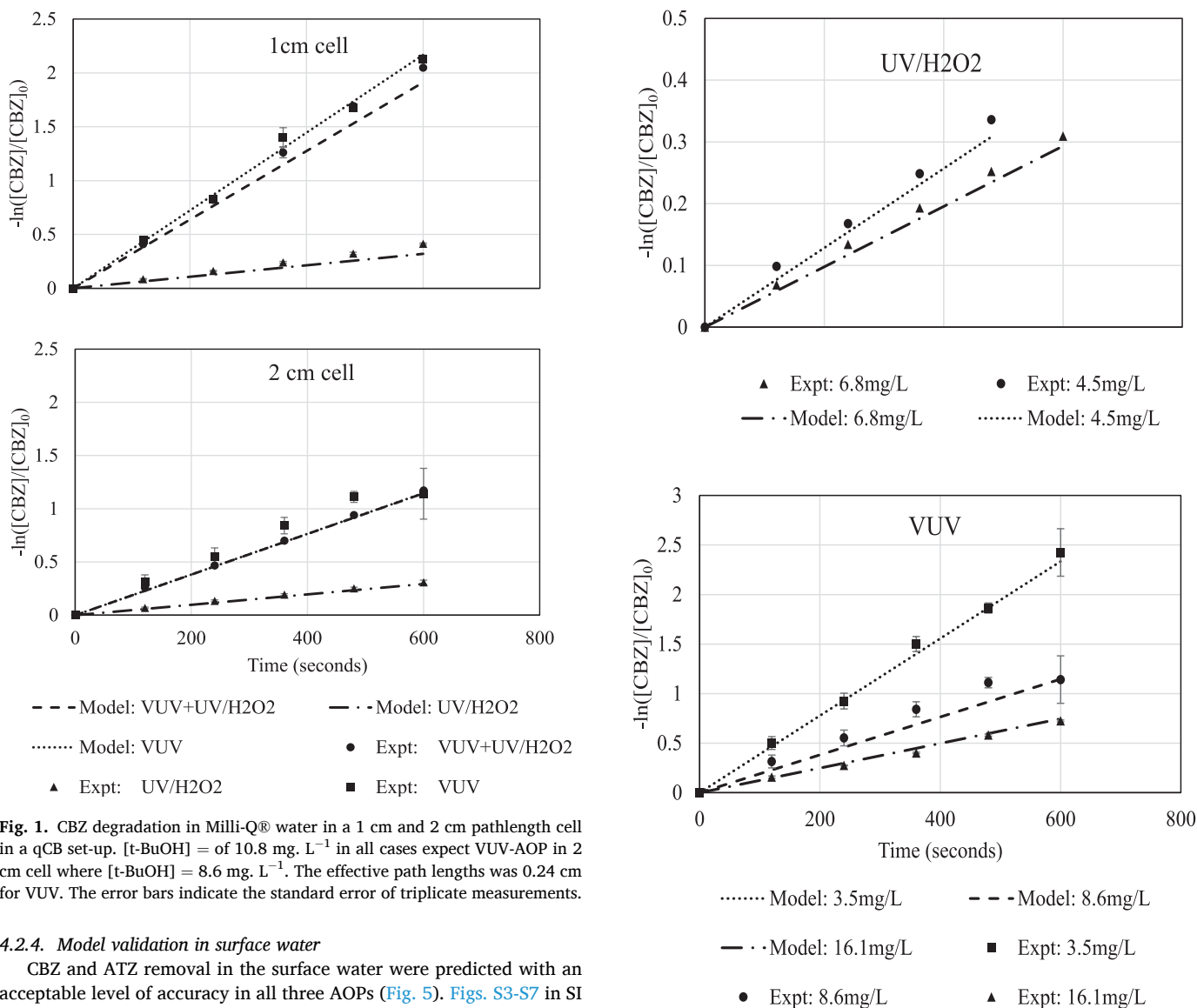
Fig. 1. CBZ degradation in Milli-Q® water in a 1 cm and 2 cm pathlength cell in a qCB set-up. [t-BuOH] = of 10.8 mg. L^{-1} in all cases expect VUV-AOP in 2 cm cell where [t-BuOH] = 8.6 mg. L^{-1}. The effective path lengths was 0.24 cm for VUV. The error bars indicate the standard error of triplicate measurements.

4.2.4. Model validation in surface water

CBZ and ATZ removal in the surface water were predicted with an acceptable level of accuracy in all three AOPs (Fig. 5). Figs. S3-S7 in SI depict the degradation of CBZ, ATZ, and DCF in surface water into which Cl$^-$ and HCO$_3^-$, CO$_3^{2-}$, NO$_3^-$, and SO$_4^{2-}$ were spiked, respectively. CBZ and ATZ are well-predicted in all cases, indicating the model's applicability to various anion concentrations. Like the original surface water and the groundwater, DCF removal is inaccurately predicted in cases with spiked anions.

When the experimental results of CBZ, ATZ, and DCF removal in spiked surface water are normalized against the original surface water matrix. A significant decrease was observed in DCF removal when [Cl$^-$] was doubled and in CBZ removal when 50 mg. L^{-1} of HCO$_3^-$ was spiked (Figure S 8). Accurate prediction of CBZ and ATZ removal in surface water spiked Cl$^-$ (Figure S 3) validates the assumption that Cl$^-$ plays an insignificant role in UV/H$_2$O$_2$ AOP in line with the findings of [51,52],

Fig. 2. CBZ degradation in ultrapure water using UV/H$_2$O$_2$ AOP and VUV-AOP in the presence of varying amounts of [t-BuOH] in a 2 cm cell in a qCB set-up. The effective path lengths were 2 cm for UV; and 0.24 cm for VUV. [H$_2$O$_2$] = 2.1×10^{-4} M. The error bars indicate the standard error of triplicate measurements.

whereas Cl$^-$ contributes towards CBZ degradation in VUV-based AOPs. Similarly, the model predicted the role of HCO$_3^-$ well in both UV/H$_2$O$_2$ and VUV-based AOPs. Hence the role of CO$_3^-$, is also well-predicted, which is essential for its applicability in natural waters.

4.2.5. Model validation in tap water matrix

Fig. 6 shows that CBZ and DCF removal in tap water matrix with and
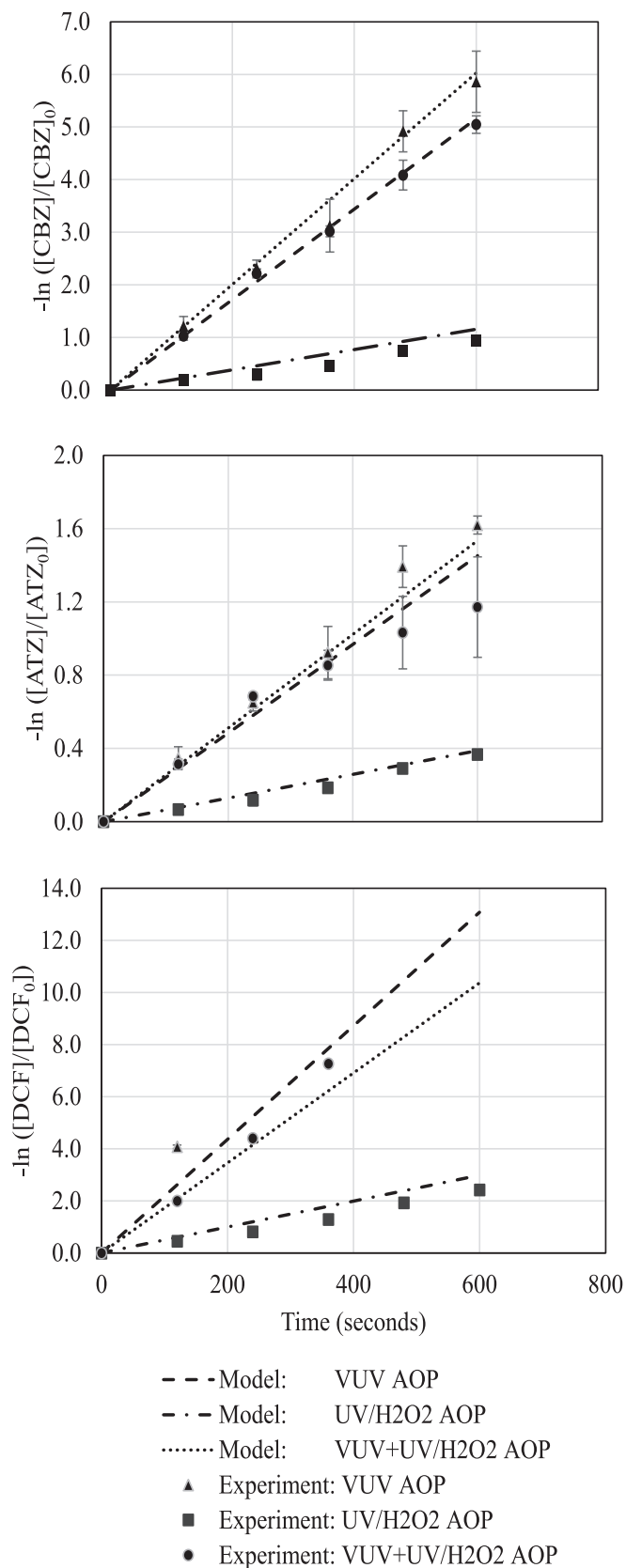
Fig. 3. CBZ, ATZ, and DCF degradation in reverse osmosis permeate three AOPs. VUV and VUV+UV/H_2O_2 AOPs were performed in 1 cm cell and UV/ H_2O_2 AOP in 2 cm cell. The effective path lengths were 2 cm for UV; and 0.24 cm for VUV. $[CBZ]_0$ = 0.08 μM, $[ATZ]_0$ = 0.1 μM and $[DCF]_0$ = 0.08 μM. $[H_2O_2]_0$ = 2.9×10^{-4} M., wherever applicable. The error bars indicate the standard error of triplicate measurements.
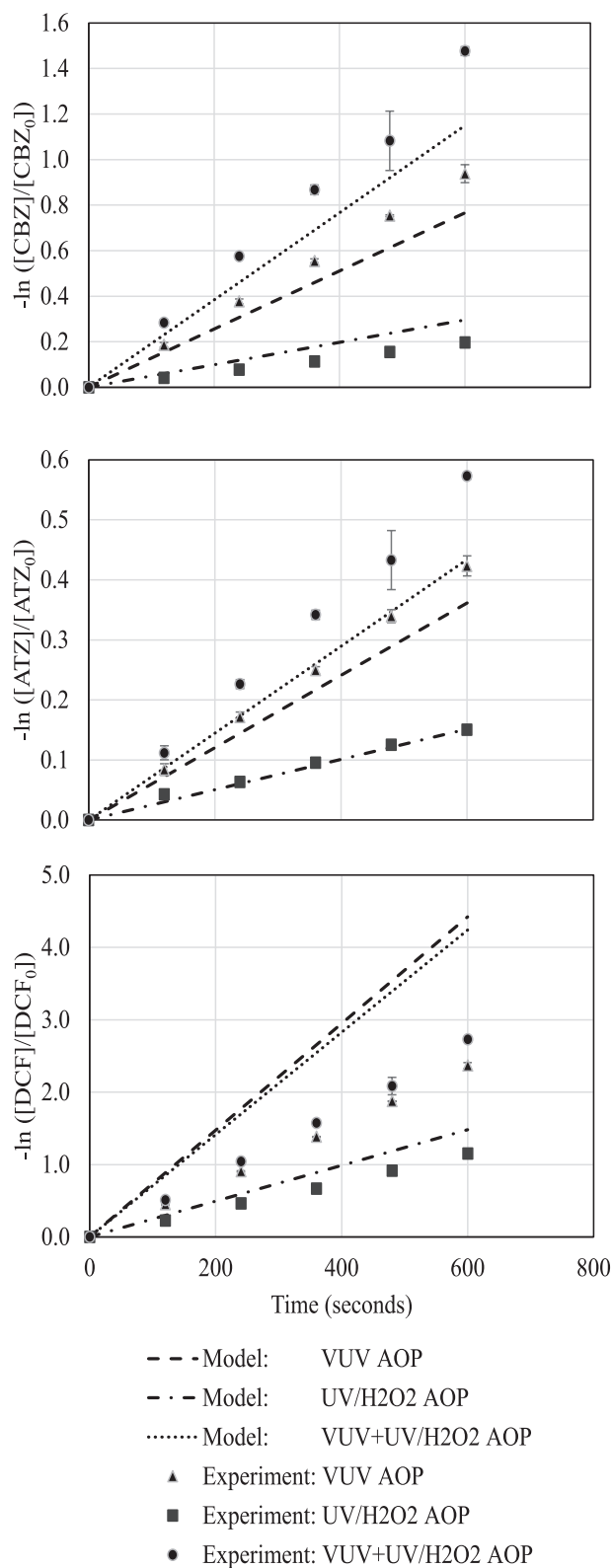
Fig. 4. CBZ, ATZ, and DCF degradation in groundwater matrix in three different AOPs. VUV and VUV+UV/H_2O_2 AOPs were performed in 1 cm cell, and UV/H_2O_2 AOP in 2 cm cell. The effective path lengths were 1.8 cm for UV; and 0.12 cm for VUV. $[CBZ]_0$ = 0.08 μM, $[ATZ]_0$ = 0.1 μM and $[DCF]_0$ = 0.08 μM. $[H_2O_2]_0$ = 2.9x10^{-4} M., wherever applicable. The error bars indicate the standard error of triplicate measurements.

without spiked Cl⁻, was well-predicted by the model. (Of note, ATZ was not spiked into this matrix). Modelling reveals that $[HO^.]_{ss}$ and $[Cl^.]_{ss}$ are the lowest in the tap water matrix (Figure S 2 in SI), explaining the lowest OMP removal. In the case of spiked [Cl⁻], the final [Cl⁻] was double the original concentration. In comparison to the effect of Cl⁻ in groundwater, the removal of CBZ and DCF in VUV+UV/H₂O₂ AOP increased by 2.5 % and 18 %, respectively. In UV/H₂O₂ AOP, there was no impact of Cl⁻ addition, in line with the findings in [51] and [58]. The model can correctly capture the effect of [Cl⁻] on both AOPs.

4.3. Industrial implications

A pilot-scale evaluation is imperative to assess the genuine efficacy of VUV AOP. For example, despite Fig. 3 illustrating a 6.2-fold increase in CBZ degradation in VUV AOP compared to UV/H₂O₂ AOP, it is crucial to note that a sub-optimal utilization of UV_{254nm} in a 2 cm path length reactor leads to an underestimation of its potential. The developed model supports dual-wavelength AOP and aids VUV piloting initiatives. The kinetic model accurately predicts CBZ and ATZ degradation in Milli-Q® and natural waters, which applies to diverse OMPs and industrial water matrices. The model requires as input the incident irradiation at UV_{254nm} and VUV_{185nm} and the constants listed in Table 2 and Table 3, which k_{R14} and k_{R18} must be experimentally determined. The model outputs OMP degradation and the concentrations of HO·, Cl·⁻ and CO₃⁻ based on specific water matrices, reactor designs, energy inputs, and H₂O₂ dosing. Several kinetic models are available to predict OMP degradation in AOPs. The novelty of the model developed in this study is that it is simple, yet robust. Its use and troubleshooting are, therefore, not restricted to modelling experts. Additionally, the model can be adapted for reactor designing in CFD platforms. The steady-state kinetic model also has the advantage of requiring lower computational resources.

Limitations of the presented kinetic model include its inapplicability for waters rich in nitrate (run-off or page from agricultural lands, some industrial water, effluent of municipal wastewater treatment plants with inefficient de-nitrification step, etc.), sulfate (water sources affected with gypsum dissolution, sewage infiltrations, industrial wastewater, etc.). In such cases, reactions involving these ions must be included in the model. Additionally, the model does not apply to high-salinity waters. High-salinity waters have high volumetric photon absorption rates, leading to very low penetration depths where mixing-related phenomena are becoming increasingly important. The high volumetric photon absorption rates also result in local radical intensities in saline waters, making the chemistry more complex. The generation and contributions Cl₂⁻ must be added to the model. In addition, the model fails to effectively forecast the removal of highly photolysis- and oxidation-susceptible compounds like DCF. However, due to their rapid degradation, this limitation is mitigated by the infrequent use of such compounds as model compounds in AOP. Further, the model is applicable in a pH range of 6–8.

5. Conclusion

A quasi-steady-state model that considers micropollutant degradation via direct photolysis at UV_{254nm} and VUV_{185nm} and oxidation via HO·, Cl·, and CO₃⁻, is developed. The model effectively predicts OMP removal in UV/H₂O₂ and VUV-based AOPs. It consistently well-predicts the natural log degradation of carbamazepine (CBZ), atrazine (ATZ), and diclofenac (DCF) across Milli-Q® water, reverse osmosis permeate, groundwater, and surface water matrices (the exception is DCF in VUV-based AOPs). CBZ, ATZ, and DCF have varying degrees of direct photolysis and oxidation susceptibility, which the model can predict well. Further, surface water and tap water matrices were spiked with various anions whose effects were also well-predicted by the model. While increased model complexity could enhance its accuracy, current predictions are deemed dependable for practical applicability. The
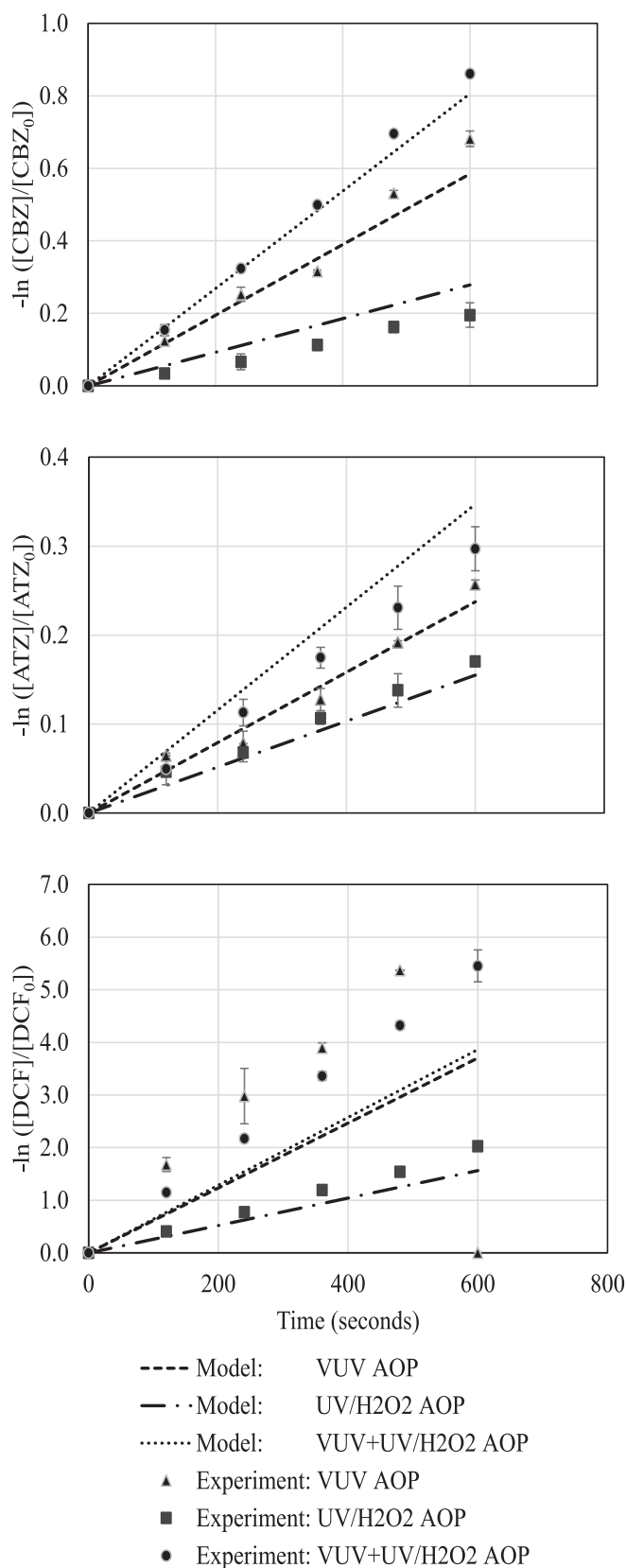
Fig. 5. CBZ, ATZ, and DCF degradation in surface water matrix in three different AOPs. VUV+UV, UV/H₂O₂, and VUV+UV/H₂O₂ AOPs were performed in a 2 cm cell. The effective path lengths were 1.8 cm for UV; and 0.02 cm for VUV. [CBZ]₀ = 0.08 μM, [ATZ]₀ = 0.1 μM and [DCF]₀ = 0.08 μM. [H₂O₂]₀ = 2.9×10⁻⁴ M., wherever applicable. The error bars indicate the standard error of triplicate measurements.
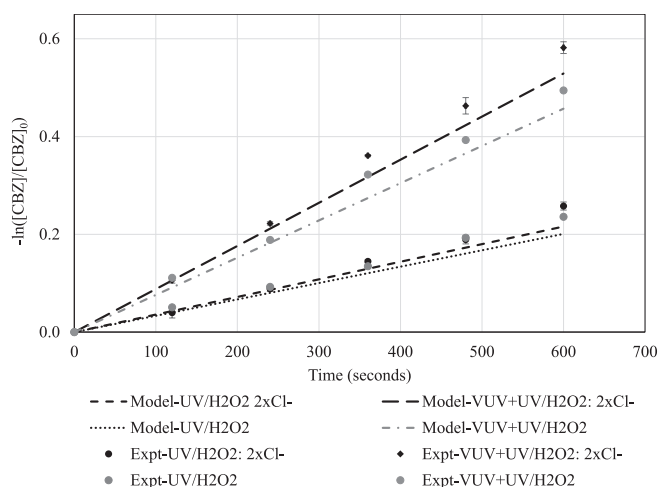
Fig. 6. Degradation of CBZ in tap water matrix in UV/H_2O_2 and VUV+UV/H_2O_2 AOPs performed in 2 cm cell at different $[Cl^-]$. $[CBZ]_0 = 0.09$ μM $[H_2O_2]_0 = 2.1 \times 10^{-4}$ M. The effective path lengths were 1.6 cm for UV; and 0.05 cm for VUV. The error bars indicate the standard error of triplicate measurements.

kinetic model can be used in CFD platforms to estimate OMP degradation in diverse photo-reactor designs, flow conditions, and irradiation. Caution is advised in cases where the water matrix contains anions dominant in VUV_{185nm} photon absorption (e.g., nitrate or sulfate); reactive species from these anions should be incorporated into the kinetic model for these waters.

CRediT authorship contribution statement

N. Kovoor George: Writing – review & editing, Validation, Supervision, Project administration, Methodology, Conceptualization. **B.A. Wols:** Writing – review & editing, Validation, Supervision, Project administration, Methodology, Conceptualization. **W. Gernjak:** Writing – review & editing, Validation, Supervision, Project administration, Methodology, Conceptualization.

Declaration of competing interest

The authors declare that they have no known competing financial interests or personal relationships that could have appeared to influence the work reported in this paper.

Data availability

Data will be made available on request.

Appendix A. Supplementary data

Supplementary data to this article can be found online at https://doi.org/10.1016/j.cej.2024.155998.

References

[1] D.B. Miklos, C. Remy, M. Jekel, K.G. Linden, J.E. Drewes, U. Hübner, Evaluation of advanced oxidation processes for water and wastewater treatment—A critical review, Water Res. 139 (2018) 118–131, https://doi.org/10.1016/j.watres.2018.03.042.

[2] Rodríguez-Chueca, J., Varella della Giustina, S., Rocha, J., Fernandes, T., Pablos, C., Encinas, Á., Barceló, D., Rodríguez-Mozaz, S., Manaia, C.M., Marugán, J., 2019. Assessment of full-scale tertiary wastewater treatment by UV-C based-AOPs: Removal or persistence of antibiotics and antibiotic resistance genes. Sci. Total Environ. 652, 1051–1061. Doi: 10.1016/j.scitotenv.2018.10.223.

[3] J.A. Mir-Tutusaus, A. Jaén-Gil, D. Barceló, G. Buttiglieri, R. Gonzalez-Olmos, S. Rodriguez-Mozaz, G. Caminal, M. Sarrà, Prospects on coupling UV/H_2O_2 with activated sludge or a fungal treatment for the removal of pharmaceutically active compounds in real hospital wastewater, Sci. Total Environ. 773 (2021) 145374, https://doi.org/10.1016/j.scitotenv.2021.145374.

[4] M. Li, W. Li, D. Wen, J.R. Bolton, E.R. Blatchley, Z. Qiang, Micropollutant degradation by the UV/H_2O_2 Process: kinetic comparison among various radiation sources, Environ. Sci. Technol. (2019), https://doi.org/10.1021/acs.est.8b06557.

[5] J.L. Weeks, G.M. Meaburn, S. Gordon, Absorption coefficients of liquid water and aqueous solutions in the far ultraviolet, Radiat. Res. 19 (1963) 559–567, https://doi.org/10.2307/3571475.

[6] G.F. Ijpelaar, D.J.H. Harmsen, E.F. Beerendonk, R.C. van Leerdam, D.H. Metz, A. H. Knol, A. Fulmer, S. Krijnen, Comparison of low pressure and medium pressure UV lamps for UV/H_2O_2 treatment of natural waters containing micro pollutants, Ozone Sci. Eng. 32 (2010) 329–337, https://doi.org/10.1080/01919512.2010.508017.

[7] Heraeus Noblelight, 2022. UV low-pressre and germicidal lamps [WWW Document]. UV lamps Syst. URL https://www.heraeus.com/en/hng/products_and_solutions/uv_lamps_and_systems/overview_uv_lamps/uv_lamps_and_systems_overview.html.

[8] M. Bagheri, M. Mohseni, Pilot-scale treatment of 1,4-dioxane contaminated waters using 185 nm radiation: Experimental and CFD modeling, J. Water Process Eng. 19 (2017) 185–192, https://doi.org/10.1016/j.jwpe.2017.06.015.

[9] N.P.F. Gonçalves, C. Medana, P. Calza, P. Roslev, Degradation of the antifungal pharmaceutical clotrimazole by UVC and vacuum-UV irradiation: kinetics, transformation products and attenuation of toxicity, J. Environ. Chem. Eng. 9 (2021) 106275, https://doi.org/10.1016/j.jece.2021.106275.

[10] N. Huang, W.-T. Shao, W.-L. Wang, Q. Wang, Z.-Q. Chen, Q.-Y. Wu, H.-Y. Hu, Removal of methylisothiazolinone biocide from wastewater by VUV/UV advanced oxidation process: kinetics, mechanisms and toxicity, J. Environ. Manage. 315 (2022), https://doi.org/10.1016/j.jenvman.2022.115107.

[11] Kiyanmehr, K., Moussavi, G., Mohammadi, S., Naddafi, K., Giannakis, S., 2022. The efficacy of the VUV/O3 process run in a continuous-flow fluidized bed reactor for simultaneous elimination of favipiravir and bacteria in aqueous matrices. Chemosphere 304. Doi: 10.1016/j.chemosphere.2022.135307.

[12] Mohammadi, S., Moussavi, G., Kiyanmehr, K., Shekoohiyan, S., Heidari, M., Naddafi, K., Giannakis, S., 2022. Degradation of the antiviral remdesivir by a novel, continuous-flow, helical-baffle incorporating VUV/UVC photoreactor: Performance assessment and enhancement by inorganic peroxides. Seperation Purif. Technol. 298. Doi: 10.1016/j.seppur.2022.121665.

[13] Y. Huang, Y. Jia, L. Zuo, Y. Huo, Y. Zhang, L. Hou, Comparison of VUV/H_2O_2 and VUV/PMS (peroxymonosulfate) for the degradation of unsymmetricaldimethylhydrazine in water, J. Water Process Eng. 49 (2022), https://doi.org/10.1016/j.jwpe.2022.102970.

[14] F. Piras, G. Nakhla, S. Murgolo, C. De Ceglie, G. Mascolo, K. Bell, T. Jeanne, G. Mele, D. Santoro, Optimal integration of vacuum UV with granular biofiltration for advanced wastewater treatment: Impact of process sequence on CECs removal and microbial ecology, Water Res. 220 (2022) 118638, https://doi.org/10.1016/j.watres.2022.118638.

[15] J.R. Bolton, K.G. Bircher, W. Tumas, C.A. Tolman, Figures-of-merit for the technical development and application of advanced oxidation technologies for both electric- and solar-driven systems (IUPAC Technical Report), Pure Appl. Chem. 73 (2001) 627–637, https://doi.org/10.1351/pac200173040627.

[16] G. Shi, S. Nishizawa, T. Matsushita, Y. Kato, T. Kozumi, Y. Matsui, N. Shirasaki, Computational fluid dynamics–based modeling and optimization of flow rate and radiant exitance for 1,4-dioxane degradation in a vacuum ultraviolet photoreactor, Water Res. 197 (2021) 117086, https://doi.org/10.1016/j.watres.2021.117086.

[17] S. Zhu, B. Dong, Y. Wu, L. Bu, S. Zhou, Degradation of carbamazepine by vacuum-UV oxidation process: Kinetics modeling and energy efficiency, J. Hazard. Mater. 368 (2019) 178–185, https://doi.org/10.1016/j.jhazmat.2019.01.043.

[18] B.A. Wols, D.J.H. Harmsen, J. Wanders-Dijk, E.F. Beerendonk, C.H.M. Hofman-Caris, Degradation of pharmaceuticals in UV LP H$_2$O$_2$ reactors simulated by means of kinetic modeling and computational fluid dynamics (CFD), Water Res. 75 (2015) 11–24, https://doi.org/10.1016/j.watres.2015.02.014.

[19] P. Xie, S. Yue, J. Ding, Y. Wan, X. Li, J. Ma, Z. Wang, Degradation of organic pollutants by Vacuum-Ultraviolet (VUV): Kinetic model and efficiency, Water Res. 133 (2018) 69–78, https://doi.org/10.1016/j.watres.2018.01.019.

[20] Y.H. Guan, J. Ma, X.C. Li, J.Y. Fang, L.W. Chen, Influence of pH on the formation of sulfate and hydroxyl radicals in the UV/peroxymonosulfate system. 9314, Environ. Sci. Technol. 45 (2011) 9308–9318, https://doi.org/10.1021/es2017363.

[21] J.C. Crittenden, S. Hu, D.W. Hand, S.A. Green, A kinetic model for H$_2$O$_2$/UV process in a completely mixed batch reactor, Water Res. 33 (1999) 2315–2328, https://doi.org/10.1016/S0043-1354(98)00448-5.

[22] A. Latifoglu, M.D. Gurol, The effect of humic acids on nitrobenzene oxidation by ozonation and O3/UV processes, Water Res. 37 (2003) 1879–1889, https://doi.org/10.1016/S0043-1354(02)00583-3.

[23] P.M. Nagarnaik, B. Boulanger, Advanced oxidation of alkylphenol ethoxylates in aqueous systems, Chemosphere 85 (2011) 854–860, https://doi.org/10.1016/j.chemosphere.2011.06.105.

[24] N. Kovoor George, B.A. Wols, D. Santoro, M. Borboudakis, K. Bell, W. Gernjak, A novel approach to interpret quasi-collimated beam results to support design and scale-up of vacuum UV based AOPs, Water Res. X 17 (2022) 100158, https://doi.org/10.1016/j.wroa.2022.100158.

[25] T. Oppenlaender, Photochemical purification of water and air. by thomas oppenländer, Angew. Chemie Int. Ed. 42 (2003) 5117, https://doi.org/10.1002/anie.200385988.

[26] J.R. Bolton, K.G. Linden, Standardization of methods for fluence (UV Dose) determination in bench-scale UV experiments, J. Environ. Eng. 129 (2003) 209–215, https://doi.org/10.1061/(asce)0733-9372(2003)129:3(209).

[27] G. Imoberdorf, M. Mohseni, Kinetic study and modeling of the vacuum-UV photoinduced degradation of 2,4-D, Chem. Eng. J. 187 (2012) 114–122.

[28] B.A. Wols, C.H.M. Hofman-Caris, D.J.H. Harmsen, E.F. Beerendonk, Degradation of 40 selected pharmaceuticals by UV/H$_2$O$_2$, Water Res. 47 (2013) 5876–5888, https://doi.org/10.1016/j.watres.2013.07.008.

[29] B. Ervens, S. Gligorovskia, H. Herrmann, Temperature-dependent rate constants for hydroxyl radical reactions with organic compounds in aqueous solutions, Phys. Chem. Chem. Phys. 5 (2003) 1811–1824, https://doi.org/10.1039/B300072A.

[30] M. Han, M. Mohseni, Impact of organic and inorganic carbon on the formation of nitrite during the VUV photolysis of nitrate containing water, Water Res. 115169 (2019), https://doi.org/10.1016/j.watres.2019.115169.

[31] Duca, C., 2015. Effect of water matrix on Vacuum UV process for the removal of organic micropollutants in surface water. University of British Columbia. Doi: 10.14288/1.0167680.

[32] H. Zhang, Q. Wu, Y. Li, S. Xiong, Simultaneous Detection of Nitrate and Nitrite Based on UV Absorption Spectroscopy and Machine Learning, Adv. UV-vis-NIR Spectrosc. 36 (2021) 38–44.

[33] J. Mack, J.R. Bolton, Photochemistry of nitrite and nitrate in aqueous solution: a review, J. Photochem. Photobiol. A Chem. 128 (1999) 1–13, https://doi.org/10.1016/S1010-6030(99)00155-0.

[34] G. Mark, H.-G.-H.-G. Korth, H.-P.-H.-P. Schuchmann, C. von Sonntag, The photochemistry of aqueous nitrate ion revisited, J. Photochem. Photobiol. A Chem. 101 (1996) 89–103, https://doi.org/10.1016/S1010-6030(96)04391-2.

[35] C.W. Wang, W.J. Zhao, B. Wu, B. Zhang, Scientific study on the celadon glaze from the Donggou kiln, China. Nucl. Instruments Methods Phys. Res. Sect, B Beam Interact. with Mater. Atoms 504 (2021) 1–5, https://doi.org/10.1016/j.nimb.2021.08.001.

[36] Yang, X., Rosario-ortiz, F.L., Lei, Y., Pan, Y., Lei, X., Westerhoff, P., 2022. Multiple Roles of Dissolved Organic Matter in Advanced Oxidation Processes. Doi: 10.1021/acs.est.2c01017.

[37] Y. Lester, C.M. Sharpless, H. Mamane, K.G. Linden, Production of photo-oxidants by dissolved organic matter during UV water treatment, Environ. Sci. Technol. 47 (2013) 11726–11733, https://doi.org/10.1021/es402879x.

[38] L. Furatian, M. Mohseni, Inuence of major anions on the 185 nm advanced oxidation process - Sulphate, bicarbonate, and chloride, Chemosphere 201 (2018) 503–510, https://doi.org/10.1016/j.chemosphere.2018.02.160.

[39] Z. Wu, K. Guo, J. Fang, X. Yang, H. Xiao, S. Hou, X. Kong, C. Shang, X. Yang, F. Meng, L. Chen, Factors affecting the roles of reactive species in the degradation of micropollutants by the UV/chlorine process, Water Res (2017), https://doi.org/10.1016/j.watres.2017.09.028.

[40] M. Han, M. Jafarikojour, M. Mohseni, The impact of chloride and chlorine radical on nitrite formation during vacuum UV photolysis of water, Sci. Total Environ. 760 (2021) 143325, https://doi.org/10.1016/j.scitotenv.2020.143325.

[41] G.V. Buxton, M. Bydder, G.A. Salmon, J.E. Williams, The reactivity of chlorine atoms in aqueous solution: part III The reactions of Cl. with solutes, Phys. Chem. Chem. Phys. 2 (2000) 237–245, https://doi.org/10.1039/A907133D.

[42] J. Barrett, M.F. Fox, A.L. Mansell, The photochemistry of aqueous sulfate ion, J. Phys. Chem. 69 (1965) 2996–3000, https://doi.org/10.1021/j100893a029.

[43] G. Imoberdorf, M. Mohseni, Degradation of natural organic matter in surface water using vacuum-UV irradiation, J. Hazard. Mater. 186 (2011) 240–246, https://doi.org/10.1016/j.jhazmat.2010.10.118.

[44] L. Wang, Q. Zhang, B. Chen, Y. Bu, Y. Chen, J. Ma, F.L. Rosario-Ortiz, R. Zhu, Some issues limiting photo(cata)lysis application in water pollutant control: critical review from chemistry perspectives, Water Res. 174 (2020) 115605, https://doi.org/10.1016/j.watres.2020.115605.

[45] Y.L. Zhang, W.L. Wang, M.Y. Lee, Z.W. Yang, Q.Y. Wu, N. Huang, H.Y. Hu, Promotive effects of vacuum-UV/UV (185/254 nm) light on elimination of recalcitrant trace organic contaminants by UV-AOPs during wastewater treatment and reclamation: a review, Sci. Total Environ. 818 (2022) 151776, https://doi.org/10.1016/j.scitotenv.2021.151776.

[46] Y. Yi, J.P. Joseph, Participation of the halogens in photochemical reactions in natural and treated waters, Molecules 22 (2017) 1684, https://doi.org/10.3390/molecules22101684.

[47] B.M. Mathew, C. Anastasio, B.M. Matthew, C. Anastasio, B.M. Mathew, C. Anastasio, A chemical probe technique for the determination of reactive halogen species in aqueous solution: part1-bromide solutions, Atmos. Chem. Phys. 6 (2006) 2423–2437, https://doi.org/10.5194/acp-6-2423-2006.

[48] G.G. Jayson, B.J. Parsons, Some simple, highly reactive, inorganic chlorine derivatives in aqueous solution, J. Chem. Soc. Faraday Trans. I 69 (1973) 1597–1607, https://doi.org/10.1039/F19736901597.

[49] G.G. Jayson, B.J. Parsons, A.J. Swallow, Some simple, highly reactive, inorganic chlorine derivatives in aqueous-solution - their formation using pulses of radiation and their role in mechanism of fricke dosimeter, J. Chem. Soc. Faraday Trans. 1 Phys. Chem. Condens. Phases 69 (1973) 1597–1607, https://doi.org/10.1039/F19736901597.

[50] Y. Li, W. Song, W. Fu, D.C.W. Tsang, X. Yang, The roles of halides in the acetaminophen degradation by UV/H$_2$O$_2$, Chem. Eng. J. (2015), https://doi.org/10.1016/j.cej.2015.02.090.

[51] Y. Gao, J. Zhang, C. Li, F. Tian, N. Gao, Comparative evaluation of metoprolol degradation by UV/chlorine and UV/H$_2$O$_2$ processes, Chemosphere 243 (2020) 125325, https://doi.org/10.1016/j.chemosphere.2019.125325.

[52] Z.H. Wu, J.Y. Fang, Y.Y. Xiang, C. Shang, X.C. Li, F.G. Meng, X. Yang, Roles of reactive chlorine species in trimethoprim degradation in the UV/chlorine process: kinetics and transformation pathways, Water Res. 104 (2016) 272–282, https://doi.org/10.1016/j.watres.2016.08.011.

[53] J.E. Grebel, J.J. Pignatello, W.A. Mitch, Effect of Halide Ions and Carbonates on Organic Contaminant Degradation by Hydroxyl Radical-Based Advanced Oxidation Processes in Saline Waters 44 (2010) 6822–6828, https://doi.org/10.1021/es1010225.

[54] X.-Y. Yu, J.R. Barker, Hydrogen peroxide photolysis in acidic aqueous solutions containing chloride ions. II. Quantum yield of HO. (Aq) radicals, J. Phys. Chem. A 107 (2003) 1325–1332, https://doi.org/10.1021/jp026666s.

[55] J. Fang, Y. Fu, C. Shang, The roles of reactive species in micropollutant degradation in the UV/free chlorine system, Environ. Sci. Technol. 48 (2014) 1859–1868, https://doi.org/10.1021/es4036094.

[56] Y. Xiang, J. Fang, C. Shang, Kinetics and pathways of ibuprofen degradation by the UV/chlorine advanced oxidation process, Water Res. 90 (2016) 301–308, https://doi.org/10.1016/j.watres.2015.11.069.

[57] A. Donati, Spectroscopic and Kinetic Investigations of Halogen Containing Radicals in the Tropospheric Aqueous Phase, University of Leipzig, Leipzig, 2002.

[58] L. Furatian, The Use of 185 nm Radiation for Drinking Water Treatment, The University of British Columbia, Environ. Prot. Agency, 2017 https://doi.org/https://10.0.55.208/1.0348109.

[59] S. Yan, Y. Liu, L. Lian, R. Li, J. Ma, H. Zhou, W. Song, Photochemical Formation of Carbonate Radical and Its Reaction with Dissolved Organic Matters, Water Res. 161 (2019) 288–296, https://doi.org/10.1016/j.watres.2019.06.002.

[60] Y. Zhou, C. Chen, K. Guo, Z. Wu, L. Wang, Z. Hua, J. Fang, Kinetics and pathways of the degradation of PPCPs by carbonate radicals in advanced oxidation processes, Water Res. 185 (2020) 116231, https://doi.org/10.1016/j.watres.2020.116231.

[61] L. Varanasi, E. Coscarelli, M. Khaksari, L.R. Mazzoleni, D. Minakata, Transformations of dissolved organic matter induced by UV photolysis, Hydroxyl radicals, chlorine radicals, and sulfate radicals in aqueous-phase UV-Based advanced oxidation processes, Water Res (2018), https://doi.org/10.1016/j.watres.2018.02.015.

[62] O.S. Keen, G. McKay, S.P. Mezyk, K.G. Linden, F.L. Rosario-Ortiz, Identifying the Factors that Influence the Reactivity of Effluent Organic Matter with Hydroxyl Radicals, Water Res. 50 (2014) 408–419, https://doi.org/10.1016/j.watres.2013.10.049.

[63] G. McKay, M.M. Dong, J.L. Kleinman, S.P. Mezyk, F.L. Rosario-Ortiz, Temperature Dependence of the Reaction between the Hydroxyl Radical and Organic Matter, Environ. Sci. Technol. 45 (2011) 6932–6937, https://doi.org/10.1021/es201363j.

[64] F.L. Rosario-Ortiz, S.P. Mezyk, D.F.R. Doud, S.A. Snyder, Quantitative Correlation of Absolute Hydroxyl Radical Rate Constants with Non-Isolated Effluent Organic Matter Bulk Properties in Water, Environ. Sci. Technol. (2008) 5924–5930, https://doi.org/10.1021/es800349b.

[65] P. Westerhoff, S.P. Mezyk, W.J. Cooper, D. Minakata, Electron Pulse Radiolysis Determination of Hydroxyl Radical Rate Constants with Suwannee River Fulvic Acid and Other Dissolved Organic Matter Isolates, Environ. Sci. Technol. 41 (2007) 4640–4646, https://doi.org/10.1021/es062529n.

[66] Y. Lei, X. Lei, P. Westerhoff, X. Zhang, X. Yang, Reactivity of Chlorine Radicals (Cl• and Cl2•−) with Dissolved Organic Matter and the Formation of Chlorinated Byproducts, Environ. Sci. Technol. 55 (2021) 689–699, https://doi.org/10.1021/acs.est.0c05596.

[67] S. Canonica, T. Kohn, M. Mac, F.J. Real, J. Wirz, U. von Gunten, Photosensitizer method to determine rate constants for the reaction of carbonate radical with organic compounds, Environ. Sci. Technol. 39 (2005) 9182–9188, https://doi.org/10.1021/es051236b.

[68] Z. Shu, J.R. Bolton, M. Belosevic, M. Gamal El Din, Photodegradation of emerging micropollutants using the medium-pressure UV/H$_2$O$_2$ Advanced Oxidation

Process, Water Res. 47 (2013) 2881–2889, https://doi.org/10.1016/j.watres.2013.02.045.

[69] Baxendale, J.H., Wilson, J.A., 1957. The photolysis of hydrogen peroxide at high light intensities. Trans. Faraday Soc. 53, 53:344–356, 1957. Doi: 10.1039/TF9575300344.

[70] G.V. Buxton, C.L. Greenstock, W.P. Helman, A.B. Ross, Critical Review of Rate Constants for Reactions of Hydrated Electrons, Hydrogen Atoms and Hydroxyl Radicals (· OH / · O-) in Aqueous Solution, J. Phys. Chem. Ref. Data 17 (1988), https://doi.org/10.1063/1.555805.

[71] Gonzalez, Oliveros, E., Wörner, M., Braun, A.M., 2004. Vacuum-ultraviolet photolysis of aqueous reaction systems. J. Photochem. Photobiol. C Photochem. Rev. 5, 225–246. Doi: 10.1016/j.jphotochemrev.2004.10.002.

[72] F.S. Dainton, P. Fowles, The photolysis of aqueous systems at 1849 Å II. Solutions containing Cl -, Br -, SO 2–4 or OH - ions, Proc. r. Soc. London. Ser. a. Math. Phys. Sci. 287 (1965) 312–327, https://doi.org/10.1098/rspa.1965.0182.

[73] G.V. Buxton, A.J. Elliot, Rate constant for reaction of hydroxyl radicals with bicarbonate ions, Radiat. Phys. Chem. 27 (1986) 241–243, https://doi.org/10.1016/1359-0197(86)90059-7.

[74] Ross, A.B., Bielski, B.H.J., Buxton, G. V, Cabelli, D.C., Helman, W.P., Huie, R.E., Grodkowski, J., Neta, P., Mulazzani, Q.G., Wilkinson, F., 1998. NDRL/NIST Solutions Kinetics Database,V3.0. NIST Stand. Ref. Database 40.

[75] L. Zhan, W. Li, L. Liu, T. Han, M. Li, Degradation of micropollutants in flow-through VUV/UV/H$_2$O$_2$ reactors: Effects of H$_2$O$_2$ dosage and reactor internal diameter, J. Environ. Sci. (2021), https://doi.org/10.1016/j.jes.2021.03.012.

[76] Ledakowicz, S., Drozdek, E., Boruta, T., Foszpańczyk, M., Olak-Kucharczyk, M., Żyłła, R., Marta, G., 2019. Impact of Hydrogen Peroxide on the UVC Photolysis of Diclofenac and Toxicity of the Phototransformation Products. Int. J. Photoenergy 2019. Doi: 10.1155/2019/1086704.

[77] Y. Lei, S. Cheng, N. Luo, X. Yang, T. An, Rate Constants and Mechanisms of the Reactions of Cl• and Cl2•– with Trace Organic Contaminants, Environ. Sci. Technol. 53 (2019) 11170–11182, https://doi.org/10.1021/acs.est.9b02462.

[78] X. Kong, L. Wang, Z. Wu, F. Zeng, H. Sun, K. Guo, Z. Hua, J. Fang, Solar irradiation combined with chlorine can detoxify herbicides, Water Res. 177 (2020) 115784, https://doi.org/10.1016/j.watres.2020.115784.

[79] S. Zhu, Z. Tian, P. Wang, W. Zhang, B. Lingjun, Y. Wu, B. Dong, S. Zhou, The role of carbonate radicals on the kinetics, radical chemistry, and energy requirement of UV/chlorine and UV/H$_2$O$_2$ processes, Chemosphere 278 (2021) 130499, https://doi.org/10.1016/j.chemosphere.2021.130499.

[80] V.J. Pereira, H.S. Weinberg, K.G. Linden, P.C. Singer, UV degradation kinetics and modeling of pharmaceutical compounds in laboratory grade and surface water via direct and indirect photolysis at 254 nm, Environ. Sci. Technol. 41 (2007) 1682–1688, https://doi.org/10.1021/es061491b.

[81] S. Canonica, L. Meunier, U. von Gunten, Phototransformation of selected pharmaceuticals during UV treatment of drinking water, Water Res. 42 (2008) 121–128, https://doi.org/10.1016/j.watres.2007.07.026.

[82] A. Serrano Mora, M. Mohseni, Temperature Dependence of the Absorbance of 185 nm photons by Water and Commonly Occurring Solutes and Its Influence on the VUV Advanced Oxidation, Environ. Sci. Water Res. Technol (2018) 16–19, https://doi.org/10.1039/C8EW00302E.